

Method of Measuring Common-Mode Current Conversion Coefficient for Estimating Variation in Radiated Emission from Printed Circuit Board Components

Cheng-Yu HO¹, Kai-Syuan CHEN¹, Tzyy-Sheng HORNG¹,
Jian-Ming WU², Chien-Hsiang HUANG³

¹ Dept. of Electrical Engineering, National Sun Yat-Sen University, No.70, Lien-Hai Rd., Kaohsiung 804, Taiwan

² Dept. of Electronic Engineering, National Kaohsiung Normal University, Kaohsiung 824, Taiwan

³ R&D Center, Realtek Semiconductor Corp.

d943010018@student.nsysu.edu.tw, d973010014@student.nsysu.edu.tw, jason@cc.nsysu.edu.tw,
jianmingwu@nknuc.nknu.edu.tw, shawn.huang@realtek.com

Abstract. *This work describes the measurement of the common-mode current conversion coefficient for a microstrip line with solid and slotted ground planes by using a VNA with a BCI probe. The radiated emissions estimated by the common-mode current conversion coefficient are further compared with those obtained by the FAC measurements. Furthermore, the proposed method was used to estimate radiated emissions from a microstrip bandpass filter. For all of the case studies, results of electromagnetic (EM) simulation demonstrate the validity of the measurement results by the proposed method. Highly promising for use in EMI measurement application, the proposed method can estimate the radiated emissions by miniaturized microstrip components on a PCB when pre-tested for compliance with EMI regulations.*

Keywords

Vector network analyzer (VNA), bulk current injection (BCI) probe, common-mode current, far-field radiated emission, microstrip components, fully-anechoic chamber (FAC), microstrip line, electromagnetic interference (EMI), printed circuit board (PCB), microstrip bandpass filters (BPFs).

1. Introduction

Radiated emissions from radio-frequency (RF) circuits are extremely complicated and difficult to evaluate. An RF circuit consists mainly of lumped elements, active devices, and microstrip components. Owing to that the dimensions of lumped elements and active devices are significantly smaller than those of the microstrip components, radiated emissions from microstrip components are generally dominant than the others, thus representing chal-

lenging topic in electromagnetic compliance. However, the radiated emissions from microstrip components on a printed circuit board (PCB) have seldom been studied. This lack of attention is owing to the predominance of common-mode radiated emissions from harness wires attached to a PCB. This situation has changed with the operating frequency reaching the gigahertz range, explaining why the microstrip component has become an efficient radiating antenna. A thorough literature review reveals that the microstrip component is a major radiated emission mechanism since it may behave similar to an antenna, subsequently radiating the noise coupled from a microstrip amplifier on a PCB [1]. Therefore, the radiated emissions from microstrip components on a PCB must be considered for high-frequency applications.

Radiated emissions can be measured in a fully-anechoic chamber (FAC), semi-anechoic chamber (SAC), or open area test site to obtain the far-field spectra for evaluating their compliance with electromagnetic interference (EMI) regulations [2]. However, such far-field spectra measurements are very expensive and time consuming. Another common method of measuring radiated emissions from a PCB uses a magnetic or electric field probe to scan the near field on the surface [3]–[5]. Although the required test setup and procedure are considerably simpler than those of far-field spectra measurements, the near-field scan results are more effective in identifying the source of radiated emissions than in estimating the levels of radiated emissions. Previous studies on quantifying the PCB radiated emission levels have been performed with the assistance of current probes [6], [7]. These studies characterized common-mode radiated emissions from a specific power-ground plane structure with a harness attached. Radiated emissions can thus be estimated based on the common-mode currents measured on the harness with a current probe. However, such current-probe measurements are limited to the power-ground plane structures with attached

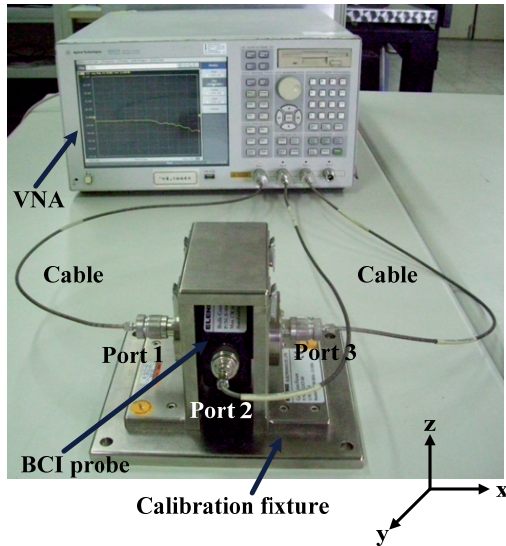


Fig. 1. Experimental setup for calibrating the transfer impedance of BCI probe using the calibration fixture.

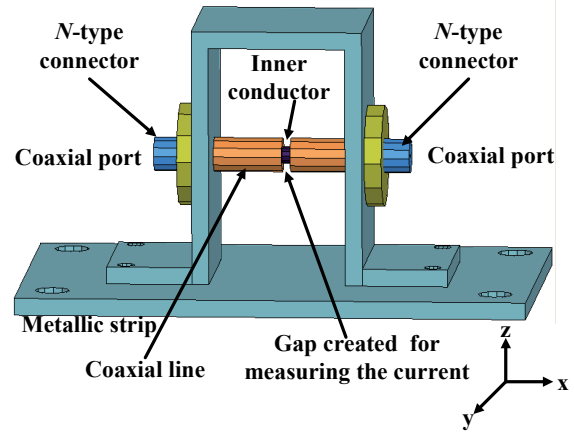


Fig. 3. Geometrical configuration of the calibration fixture.

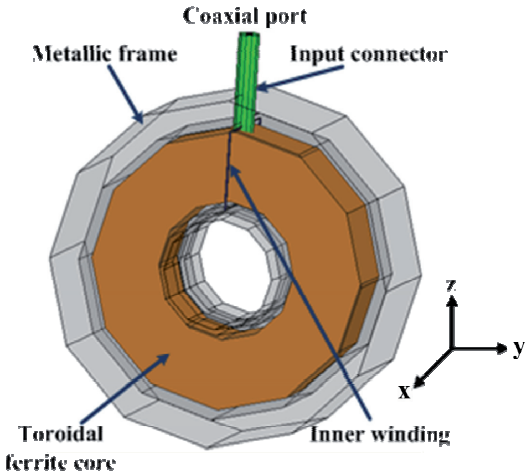


Fig. 2. Geometrical configuration of the BCI probe.

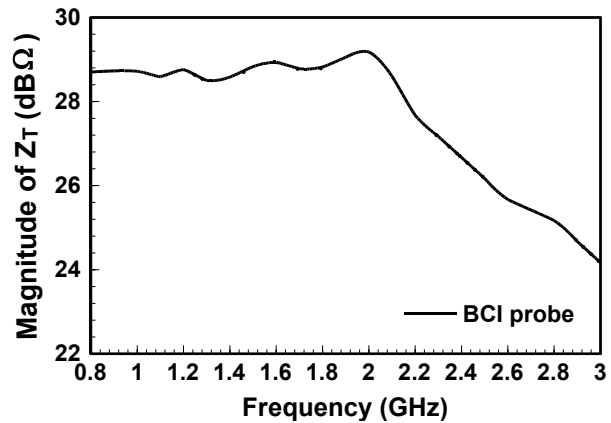


Fig. 4. Magnitude of the BCI probe transfer impedance by using the calibration setup shown in Fig. 1.

harness for estimating their effects on radiated emissions. In fact, PCBs for wireless electronic products contain many microstrip components that radiate like an antenna at high frequencies, which still cannot be evaluated with current probe-based measurements.

In recent years, the network analyzer measurements have been used in electromagnetic compatibility (EMC) application to measure S-parameters, which correlate with the electromagnetic emission and susceptibility [8], [9]. Moreover, bulk current injection (BCI) probes have also proven effective for characterizing radiation-induced effects in conducted susceptibility tests [10]. Considerable effort has thus focused recently on calibrating BCI probes with network analyzers [11]. Given these developments, this work proposes a novel method for measuring common-mode radiated emissions from microstrip components on a PCB. Importantly, the proposed method is highly promising for use as a pre-test of a PCB for compliance with EMI regulations.

2. Calibration of BCI Probe

This work demonstrates the feasibility of using a network analyzer and BCI probe to measure the common-mode conversion coefficients of microstrip components for estimating the radiated emissions in the far field. Measurement accuracy of common-mode conversion coefficients is also ensured by implementing a calibration procedure for the BCI probe, an F-150 model made by Fischer Custom Communication [13], [14]. Notably, the BCI probe is designed for operating frequencies ranging from 0.8 to 2.1 GHz and has been extended to operate up to 3 GHz in this work. Therefore, the calibration of the BCI probe is carried out to determine the frequency-dependent transfer

impedance in the 0.8-3 GHz frequency range. Fig. 1 shows the experimental setup for calibrating transfer impedance of the BCI probe when mounted in a calibration fixture [12].

Figs. 2 and 3 schematically depict the geometrical configuration of the BCI probe and the calibration fixture, respectively. According to these figures, the BCI probe comprises a donut-shaped metallic housing, toroidal ferrite core, winding coil and coaxial connector, whereas the calibration fixture consists of a coaxial line, pair of coaxial connectors and U-shaped metal piece screwed onto a rectangular metal piece. Notably, there is a 2-mm wide annular gap and a 5-mm wide annular slot on the outer conductor of the coaxial line and the inner ring of the donut-shaped metallic housing, respectively, to allow for measurement of the inner conductor current by the BCI probe.

Fig. 1 describes the connection of the BCI probe mounted in the calibration fixture to the three ports of network analyzer. Port 1 is connected to the coaxial connector of the calibration fixture; port 2 is connected to the coaxial connector of the BCI probe, and port 3 is connected to the other coaxial connector of the calibration fixture. Excitation from port 1 generates a current on the coaxial line that induces a voltage at port 2, the BCI probe output, when port 3 is terminated by a matched load. Transfer impedance is defined as the BCI probe output current I_1 , as calculated by

$$Z_T(\omega) = \frac{V_2(\omega)}{I_1(\omega)} = S_{21,cal}(\omega)Z_0 \quad (1)$$

where $S_{21,cal}$ denotes the transmission parameter from port 1 to port 2 in the calibration measurement, and Z_0 denotes 50 Ω. Owing to (1), the BCI probe has a frequency-dependent transfer impedance ranging from 24 to 29 dBΩ in the frequency range of 0.8-3 GHz, as shown in Fig. 4.

3. Radiated Emissions from Microstrip Line

Common-mode currents on the conductors represent the main radiation factor in microstrip components [15], [16]. For an ideal microstrip line with infinite ground plane, no ground inductance occurs, explaining why the radiated emissions are only from the microstrip-mode currents out of phase between the signal and ground conductors. However, for a practical microstrip line with finite ground plane, as shown in Fig. 5(a), parasitic ground inductance occurs, which subsequently producing a voltage drop when the return current flows through the finite ground plane. Additionally, the finite ground plane with a zero potential is maintained by inducing a voltage on the finite plane to cancel out that voltage drop. However, a by-product of this induced voltage is to excite a ground current in phase with the signal current, resulting in the common-mode currents. Fig. 5(b) shows a microstrip line with

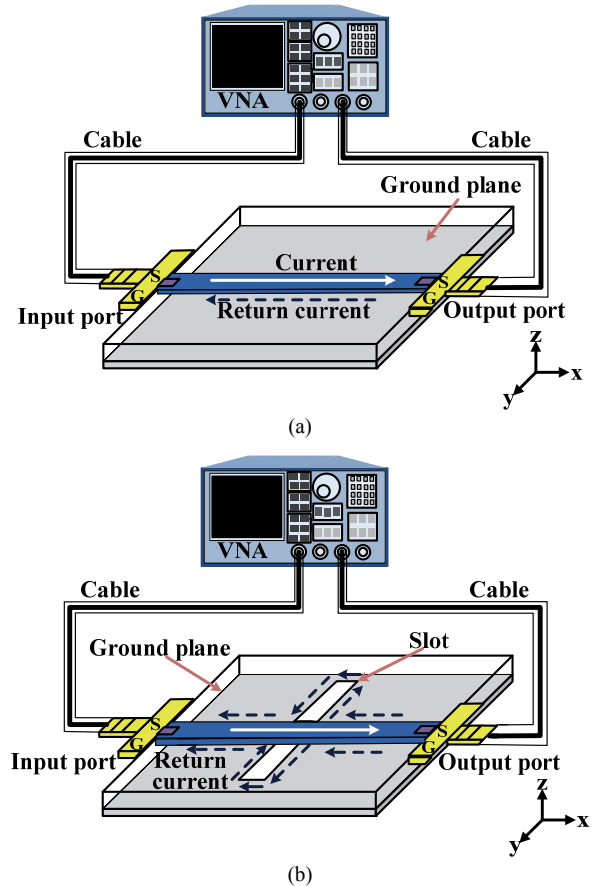


Fig. 5. Radiated emissions caused by a microstrip line with different ground planes. (a) Solid ground plane. (b) Slotted ground plane.

a slotted ground plane. The corresponding parasitic ground inductance is larger than that of Fig. 5(a), owing to a longer path for the return current to flow around the slot on the ground plane. The resulting common-mode current in Fig. 5(b) is thus more significantly increased than that in Fig. 5(a).

Fig. 6 shows a microstrip line inserted into the center hole of the BCI probe for measuring the common-mode conversion coefficients with a network analyzer. With similar port connections in the calibration procedure, port 1, 2, and 3 of the network analyzer are connected to the microstrip-line input, BCI probe output and microstrip-line output, respectively. Notably, the microstrip line is parallel to the x-axis in the Cartesian coordinate system, and the BCI probe is oriented perpendicularly to the x-axis in order to measure the magnetic field around the x-axis. With excitation, the magnetic fields produced by the out-of-phase (microstrip-mode) currents on the signal and ground conductors cancel out each other within the BCI probe, while those produced by the in-phase (common-mode) currents induce a voltage on the BCI probe output.

Figs. 7(a) and 7(b) show the EM simulation models that use a high permeability loop to imitate the magnetic field coupling mechanism of the BCI probe. The loops are set with high permeability ($\mu_r = 1000$) to behave as a magnetic circuit to carry the magnetic flux induced due to com-

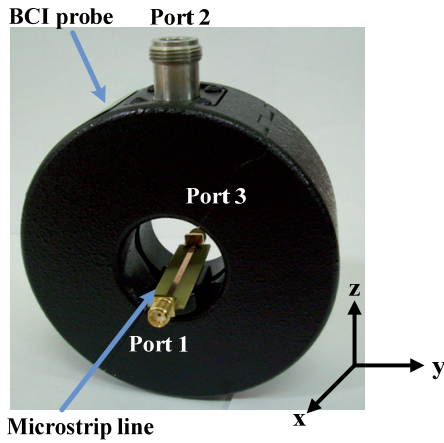


Fig. 6. Experimental setup for measuring the common-mode conversion coefficient of the microstrip lines with different ground planes.

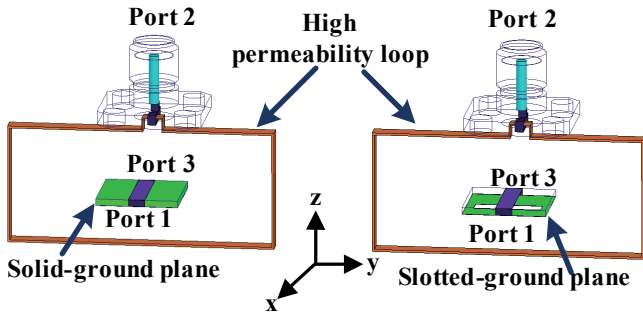


Fig. 7. EM simulation configuration for obtaining the common-mode conversion coefficient of the microstrip lines with different ground planes. (a) Solid ground plane. (b) Slotted ground plane.

mon-mode current on the microstrip component. The magnetic flux further induces currents on center conductor of the coaxial connector that is terminated by a 50 Ω load. A voltage drop across the load is thus determined in proportion to the common-mode current. The common-mode currents can be estimated in terms of the transmission coefficient S_{21} and the loop transfer impedance Z_T as follows:

$$I_{CM}(\omega) = \frac{S_{21}(\omega)}{Z_T(\omega)} V_{in} \quad (2)$$

where V_{in} denotes the input voltage wave amplitude of the microstrip line.

The transmission coefficient S_{21} in (2) can be treated as a conversion coefficient from microstrip mode to common mode. Consequently, Fig. 8 compares the measured and simulated common-mode conversion coefficients of the microstrip lines with a solid or slotted ground plane. Notably, the microstrip lines in this study are on a 0.8-mm thick FR4 substrate with a characteristic impedance of 50 Ω, having a length of 10 mm and a width of 2 mm. The width of the finite ground plane is 5 mm, while the slot on the finite ground plane is 4 mm long and 2 mm wide. Fig. 8 shows a reasonable agreement between the proposed method and EM simulation over the entire studied frequency range. To achieve a satisfactory agreement, the

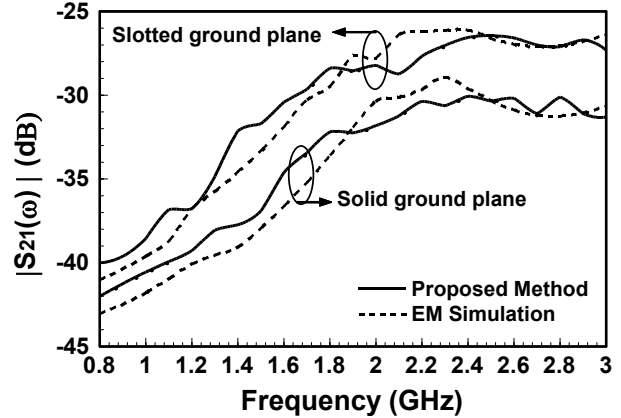


Fig. 8. Comparison of common-mode conversion coefficient magnitudes of the microstrip line with different ground planes between the proposed method and EM simulation.

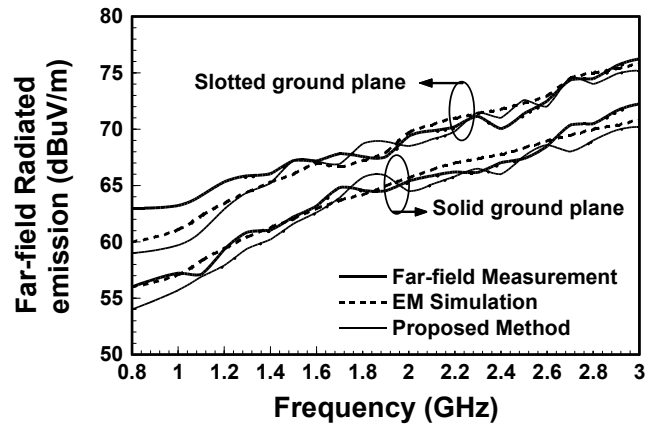


Fig. 9. Comparison of far-field radiated emissions from the microstrip line with different ground planes obtained in a fully-anechoic chamber with predictions by the proposed method and EM simulation.

proposed high permeability loop model in the EM simulation must be calibrated beforehand to have the same transfer impedance as that of the BCI probe. According to Fig. 8, the slotted-ground microstrip structure has an approximately 5 dB higher transmission coefficient than that of the solid-ground microstrip structure in the studied frequency range of 0.8-3 GHz. By assuming a uniform common-mode current distribution in the microstrip components, the Hertzian dipole model can be used to estimate the far-field radiated emissions from the components, as given by [17]

$$|E_{Cmax}(\omega)| = 4\pi \times 10^{-7} \frac{I_{CM}(\omega) \cdot L \cdot \omega \cdot \cos(\frac{1}{2}\beta h)}{2\pi R} \quad (3)$$

where L denotes the length of the signal trace, h denotes the thickness of microstrip substrate, β denotes the phase constant of free space, and R denotes the distance between the measurement point and the microstrip component.

For validation, radiated emissions at 1 m distance are estimated by (3) at an input power of 0 dBm (i.e., $V_{in} = 224$ mV) and compared with the FAC measurement results

and the EM simulation results using Ansys-Ansoft HFSS, as shown in Fig. 9. This comparison reveals satisfactory correlation among the three approaches. Notably, in the FAC measurement ferrite cores are used to suppress the common-mode current on each cable for removing the radiation from the cables. Fig. 9 also compares the radiated emission results between the slotted-ground microstrip structure and the solid-ground microstrip structure. Coinciding with the difference of the common-mode conversion coefficients in Fig. 8, the former structure has approximately a 5 dB higher radiated emission than the latter structure in the frequency range of study.

Above experimental validation and discussion suggests that the EMI source results mainly from the defected PCB ground plane. It should be noted that for the simulation and measurement results shown in Fig. 8, the central cross section of the microstrip component is aligned to the central longitudinal section of the annular slot in the inner ring of the BCI probe. Therefore, the far-field radiated emission data obtained by the proposed method can be regarded as due to a spatial average of the common-mode current flowing inside the center hole of the BCI probe. Moreover, the noise floor of the network analyzer measurement with a BCI probe and the far-field radiated emission measurement in FAC is around -70 dB and 20 dB μ V, respectively.

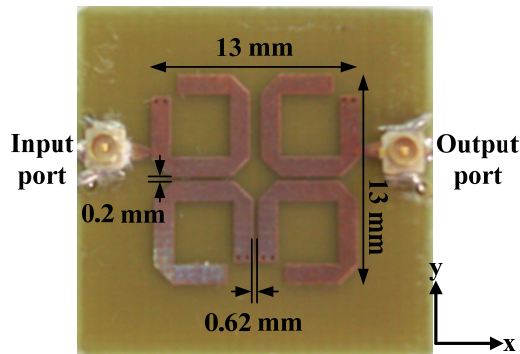


Fig. 10. Top view dimensions of four-order microstrip quasi-elliptic bandpass filter implemented on the FR4 substrate.

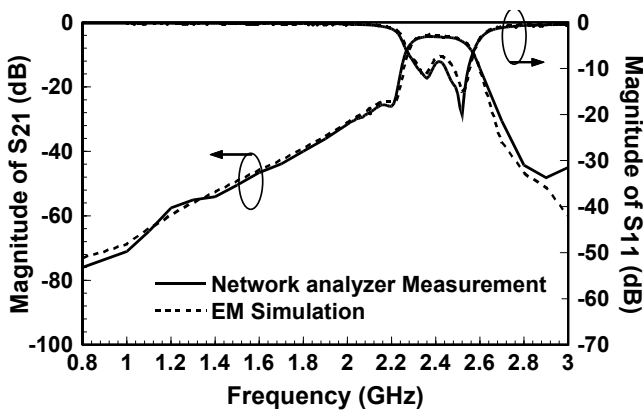


Fig. 11. Comparison of return loss and insertion loss of the microstrip bandpass filter between network analyzer measurement and EM simulation.

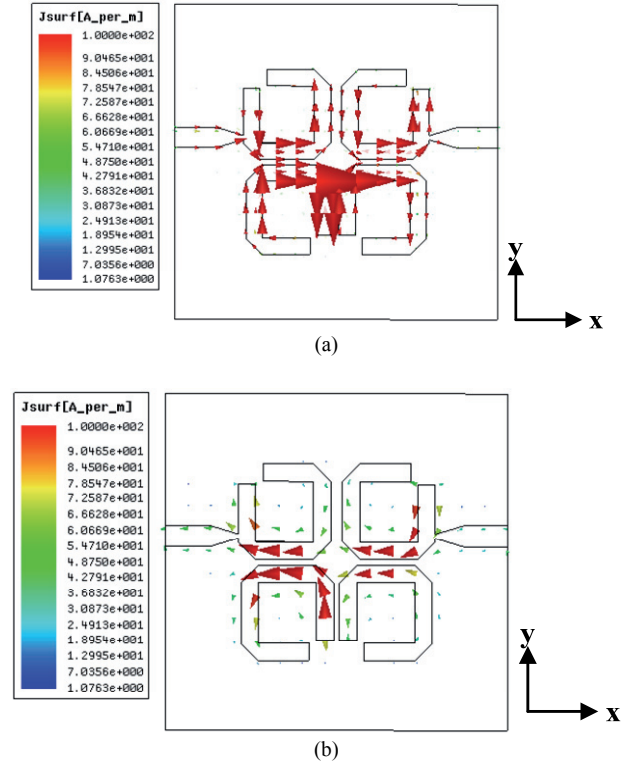


Fig. 12. Simulated surface current density distribution of microstrip bandpass filter at the frequency of 2.4 GHz. (a) Signal trace. (b) Ground plane.

4. Radiated Emissions from Microstrip Bandpass Filter

Microstrip bandpass filters are crucial components in suppressing the output harmonics in a transmitter and input interferences in a receiver. Often constructed by coupling of resonators, their passband occurs close to resonant frequencies of the resonators, at which, electromagnetic radiation is easily emitted. Therefore, this work heavily emphasizes use of the proposed method in evaluating the radiated emissions from microstrip bandpass filters. Fig. 10 shows a 2.4 GHz microstrip bandpass filter implemented on a 0.8-mm thick FR4 substrate. In this work, the filter is designed based on a fourth-order quasi-elliptic prototype and then constructed by coupling four microstrip open-loop resonators [18]. The overall occupied area is 13 \times 13 mm². Fig. 11 compares the simulated and measured magnitudes of S_{11} and S_{21} parameters over the entire studied frequency range. Notably, the designed microstrip filter has an insertion loss lower than 3.4 dB and a return loss higher than 10 dB in the 2.4-2.5 GHz passband. Fig. 12(a) and 12(b) illustrate the simulated surface current distribution on the signal trace and ground plane, respectively, of the microstrip bandpass filter at 2.4 GHz. The current distribution of a microstrip bandpass filter is generally decomposed into x- and y-directed components. The magnitude of surface current distribution of x-directed component is obviously larger than that of the y-directed component.

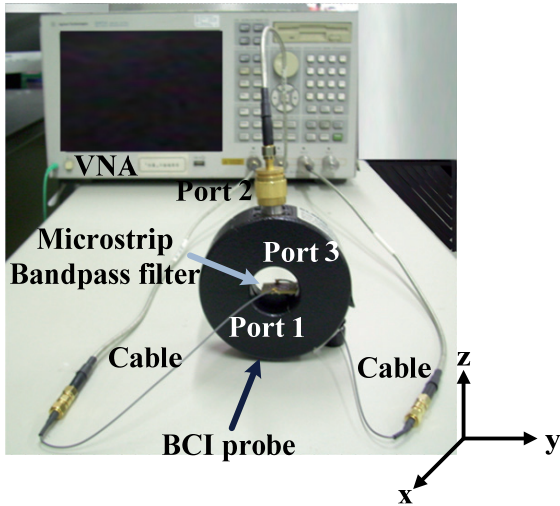


Fig. 13. Experimental setup for measuring the common-mode conversion coefficient of the microstrip bandpass filter.

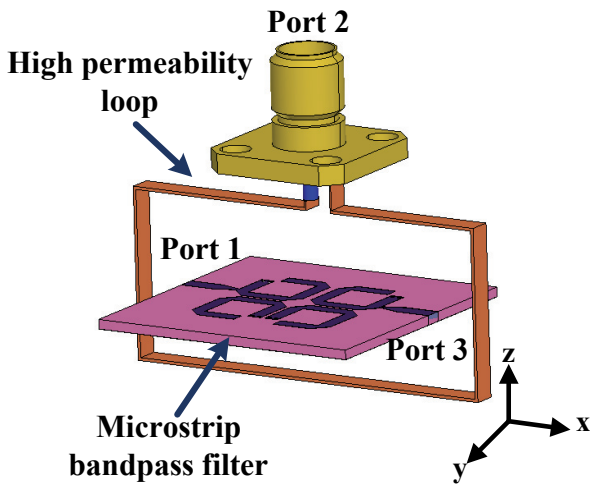
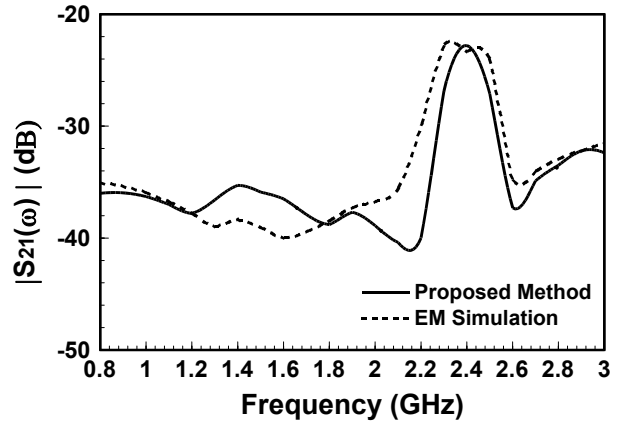


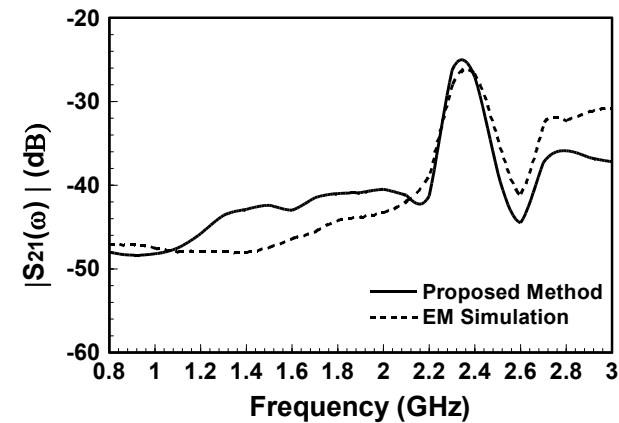
Fig. 14. EM simulation configuration for obtaining the common-mode conversion coefficient of the microstrip bandpass filter.

Fig. 13 demonstrates the feasibility of using the BCI probe to measure the common-mode conversion coefficients of the x- and y-directed current components in the microstrip bandpass filter with a network analyzer. The common-mode currents on the microstrip bandpass filter apparently have both the x- and y-directed components. According to Ampere’s circuital law, the x-directed component and the y-directed component produce the magnetic fields around the x-axis and the y-axis, respectively. Therefore, the BCI probe oriented perpendicularly to the x-axis can measure the magnetic field induced by the x-directed current component. Then, by rotating the BCI probe by 90°, the BCI probe is oriented perpendicularly to the y-axis, allowing for measurement of the magnetic field induced by the y-directed current component.

For validation, the common-mode current on the microstrip bandpass filter is investigated using the EM modeling of the high permeability loop. Fig. 14 shows EM modeling of the high permeability loop for determining the



(a)



(b)

Fig. 15. Comparison of common-mode conversion coefficient magnitudes of the microstrip bandpass filter between the proposed method and EM simulation. (a) Filter oriented in x-axis. (b) Filter oriented in y-axis.

magnetic field induced by the y-directed common-mode current component. By a 90° rotation of microstrip bandpass filter, the high permeability loop can also determine the magnetic field induced by the x-directed common-mode current component. Fig. 15(a) and 15(b) respectively show the measured common-mode conversion coefficient of x-directed and y-directed component. The x-directed component has an average of about 6 dB higher common-mode conversion coefficient than the y-directed component with respect to the frequency range of study. Fig. 15(a) and 15(b) also compare the common-mode conversion coefficient obtained by the proposed method and by EM simulation. Comparing the results from both approaches reveals an acceptable agreement throughout the measurement frequency range.

With (2) and (3), the two common-mode current components in the microstrip bandpass filter and their respective radiated emissions in the far field can be obtained. The overall radiated emissions can be evaluated by taking the root of the sum of the square of each of these respective radiated emissions. Consequently, Fig. 16 compares the evaluated far-field radiated emissions by using the proposed method with the measurement results from the FAC

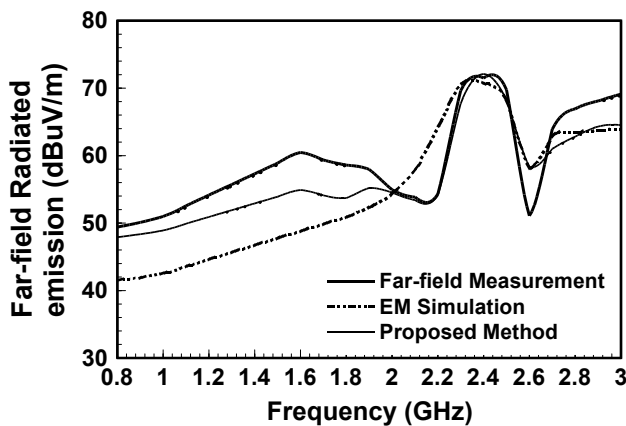


Fig. 16. Comparison of radiated emissions from the microstrip bandpass filter obtained in a fully-anechoic chamber with predictions by the proposed method and EM simulation.

and the simulation ones by HFSS. This comparison indicates a sufficient correlation in the passband frequencies of the microstrip bandpass filter. Notably, in this comparison the input power to the microstrip bandpass filter is 0 dBm. Fig. 16 reveals that the strongest radiation from the microstrip bandpass filter occurs in the passband because of the use of open-loop resonators with a resonant frequency close to the passband. These open-loop resonators usually generate strong common-mode radiation at resonance.

Although this study is focused on predicting the radiated emissions from two-port microstrip components, the proposed method can be extended to pre-compliance EMI test of a miniaturized PCB for an RF module in multi-port configuration with the help of a multi-port network analyzer.

5. Conclusion

This work proposes a novel method for using a network analyzer with a BCI probe to measure the common-mode conversion coefficient for estimating radiated emissions from a microstrip component. Additionally, the far-field radiated emission predictions obtained by the proposed method for a microstrip component are compared with EM simulations and FAC measurements. Study examples include a microstrip line with solid and slotted ground planes and a microstrip bandpass filter, showing a good agreement among the different approaches.

Acknowledgements

The authors wish to thank the Automotive Research and Testing Center, Taiwan, for supporting the FAC measurements in this research.

References

- [1] HSIEH, H.-C., CHIU, C.-N., WANG, C.-H., CHEN, C.-H. A new approach for fast analysis of spurious emissions from RF/microwave circuits. *IEEE Transactions Electromagnetic Compatibility*, 2009, vol. 51, no. 3, p. 631 - 638.
- [2] KWON, J.H., CHOI, H.D. Experimental verification of correlation algorithm between FAC and open area test site/SAC. In *IEEE International Symposium Electromagnetic Compatibility*. Boston (USA), 2003, p. 910 - 914.
- [3] FIORI, F., MUSOLINO, F. Comparison of IC conducted emission measurement methods. *IEEE Transactions Instrument Measurement*, 2003, vol. 52, no. 3, p. 839 - 845.
- [4] BAUDRY, D., ARCHAMBAL, C., LOUIS, A., MAZARI, B., EUDELIN, P. Applications of the near-field techniques in EMC investigations. *IEEE Transactions Electromagnetic Compatibility*, 2007, vol. 49, no. 3, p. 485 - 493.
- [5] VIVES-GILABERT, Y., ARCHAMBAL, C., LOUIS, A., DARAN, F., EUDELIN, P., MAZARI, B. Modeling magnetic radiations of electronic circuits using near-field scanning method. *IEEE Transactions Electromagnetic Compatibility*, 2007, vol. 49, no. 2, p. 391-400.
- [6] HOCKANSON, D. M., DREWNIK, J. L., HUBING, T. H., LAM, C. W. Quantifying EMI resulting from finite-impedance reference planes. *IEEE Transactions Electromagnetic Compatibility*, 1997, vol. 39, no. 4, p. 286 - 297.
- [7] HOCKANSON, D. M., DREWNIK, J. L., HUBING, T. H., VAN DOREN, T. P., WILHELM, M. J. Investigation of fundamental EMI source mechanisms driving common-mode radiation from printed circuit boards with attached cables. *IEEE Transactions Electromagnetic Compatibility*, 1996, vol. 38, no. 4, p. 557 - 566.
- [8] CHEN, C. Examination of electronic module immunity using transfer functions. In *IEEE International Symposium Electromagnetic Compatibility*. Chicago (USA), 2005, p. 756-761.
- [9] CHEN, K.-S., HORNG, T.-S., HO, C.-Y., WU, J.-M., PENG, K.-C. Diagnosis of EMI to laptop WWAN device from TFT-LCD driver using non-contact measurement-based transfer function technique. In *IEEE International Symposium Electromagnetic Compatibility*. Fort Lauderdale (USA), 2010, p. 301 - 304.
- [10] *Road Vehicles - Component Test Methods for Electrical Disturbances from Narrowband Radiated Electromagnetic Energy - Part 4: Bulk Current Injection (BCI)*. ISO Standard 11452-4, 2005.
- [11] GRASSI, F., MARLIANI, F., PIGNARI, S. A. Circuit modeling of injection probes for bulk current injection. *IEEE Transactions Electromagnetic Compatibility*, 2007, vol. 49, no. 3, p. 563 - 576.
- [12] HO, C.-Y., CHEN, K.-S., HORNG, T.-S. Estimating reduction of radiated emission from microstrip components using vector network analyzer with a Bulk Current Injection probe. *IEEE Microwave and Wireless Components Letters*, 2013, vol. 23, no. 2, p. 118 - 110.
- [13] *F-150 Injection Current Probe Characterization*: Fischer Custom Communication Inc., 2006.
- [14] CHUNDRU, R., CHANDRA, S. A new test setup and method for the calibration of current clamps. *IEEE Transactions Electromagnetic Compatibility*, 2005, vol. 47, no. 2, p. 335 - 343.
- [15] CHEN, I.-F., HSUE, C.-W. Novel model for the estimation of radiation emission from printed circuit boards with narrow ground pattern. *Microwave Optical Technology Letters*, 2002, vol. 33, no. 5, p. 332 - 335.

- [16] SU, C., HUBING, T. H. Imbalance difference model for common-mode radiation from printed circuit boards. *IEEE Transactions Electromagnetic Compatibility*, 2011, vol. 53, no. 1, p. 150 - 156.
- [17] PAUL, C. R. A comparison of the contributions of common-mode and differential-mode currents in radiated emissions. *IEEE Transactions Electromagnetic Compatibility*, 1989, vol. 31, no. 2, p. 189 - 193.
- [18] VAGNER, P., KASAL, M. A novel bandpass filter using a combination of open-loop defected ground structure and half-wavelength microstrip resonators. *Radioengineering*, 2010, vol. 19, no. 3, p. 392 - 396.

About Authors ...

Cheng-Yu HO was born on September 12, 1977, in Kaohsiung, Taiwan. He received the B.S.E.E. and M.S.E.E. degrees from the National ChangHua University of Education, ChangHua, Taiwan, in 2002 and 2004, and Ph.D. degree from National Sun Yat-Sen University, Kaohsiung, Taiwan, in 2013. He is currently a Research and Development Engineer with the Research and Development Electrical Laboratory, Advance Semiconductor Engineering (ASE), in charge of system-in-package (SiP) circuit design and analysis. His main research interests include design and modeling of RF/microwave integrated passive devices, analysis and testing technologies of electromagnetic compatibility (EMC) problems of electronic systems and integrated circuits.

Kai-Syuan CHEN (S'10) was born in Kaohsiung, Taiwan, in 1984. He received the B.S. degree in Electrical Engineering from the National University of Kaohsiung, Kaohsiung, Taiwan, in 2006, and the M.S. degree in Communication Engineering from the National University of Tainan, Tainan, Taiwan, in 2008. He is currently working toward the Ph.D. degree in Electrical Engineering at National Sun Yat-sen University, Kaohsiung, Taiwan. His research interests include near-field electromagnetism, contactless measurements, and radio frequency signal integrity (RFSI).

Tzyy-Sheng HORNG was born in Taichung, Taiwan, on December 7, 1963. He received the B.S.E.E. degree from the National Taiwan University, Taipei, Taiwan, in 1985, and the M.S.E.E. and Ph.D. degrees from the University of

California at Los Angeles (UCLA), in 1990 and 1992, respectively. Since August 1992, he has been with the Department of Electrical Engineering, National SunYat-Sen University, Kaohsiung, Taiwan, where he was the Director of the Telecommunication Research and Development Center (2003–2008) and Director of the Institute of Communications Engineering (2004–2007), and where he is currently a Professor and the Advanced Semiconductor Engineering Inc. (ASE Inc.) Chair Professor. He has authored or coauthored over 100 technical publications published in IEEE journals and conferences proceedings. He holds over ten patents. His research interests include RF and microwave integrated circuits and components, RF signal integrity for wireless system-in-package, digitally assisted RF technologies, and green radios for cognitive sensors and Doppler radars.

Jian-Ming WU was born November 13, 1974, in Kaohsiung, Taiwan. He received the B.S.E.E degree from the Yuan Ze University, Chungli, Taiwan, in 1997, and the M.S.E.E. and Ph.D. degrees from the National Sun Yat-Sen University, Kaohsiung, Taiwan, in 2000 and 2006, respectively. He joined the Graduate Institute of Communication Engineering, National University of Tainan, Tainan, Taiwan, as an Assistant Professor in August 2006. In August 2007, he joined the Department of Electronic Engineering, National Kaohsiung Normal University, Kaohsiung, Taiwan, as an Assistant Professor and was promoted to Associate Professor in March 2012. His current research interests include design of monolithic microwave integrated circuit, modeling of RF components, and chip-package-board codesign. He was the recipient of the 2006 National Sun Yat-Sen University Outstanding Doctoral Dissertation Award. Since 2006, he has been serving on the IC Implementation Review Committee, National Chip Implementation Center, Hsinchu, Taiwan.

Chien-Hsiang HUANG was born on August 24, 1978, in Kaohsiung, Taiwan. He received the B.S.E.E., M.S.E.E., and Ph.D. degrees from National Sun Yat-Sen University, Kaohsiung, Taiwan, in 2000, 2002, and 2011, respectively. He is currently a Research and Development Engineer with the Realtek Semiconductor Corporation, HsinChu, Taiwan. His main research interests are design and modeling of RF/microwave integrated passive devices.